Closed-Loop Identification of a Continuous Crystallization Process

R. A. Eek, J. A. Both, and P. M. J. Van den Hof
Mechanical Engineering Systems and Control Group, Delft University of Technology, Mekelweg 2, 2628 CD Delft, The Netherlands

Identification of low-order linear multiinput/multioutput models can lead to accurate descriptions of the dynamic behavior of a continuous crystallization process. While open-loop experiments exhibit an oscillating crystal size distribution, improved experimental conditions can be established through stabilization of the process with a simple single-loop feedback controller. The resulting closed-loop identification problem is studied using low-order linear multivariable input–output models. Two closed-loop identification methods are applied, one of which was recently introduced to provide accurate approximate models in general closed-loop process configurations. Identification and validation data are obtained from an evaporative pilot crystallizer, and the identified models are validated in terms of time- and frequency-domain responses. A fourth-order, three-input three-output model is shown to describe accurately the process dynamics. The results are compared with a linearized and reduced first-principles model.

Introduction

Crystallization from solution is a well-established industrial purification and separation process, in which a solids fraction is derived from a solution. In volume this unit operation is second to distillation. Examples of substances produced on a large scale, with production rates exceeding 10^6 ton/yr, are bulk inorganic materials like sodium chloride, and ammonium-sulphate (a fertilizer), and organic materials like adipic acid (a raw material for nylon).

A main characteristic of crystallization processes is that a distribution of differently sized particles is produced, which is characterized by the *crystal-size distribution* (CSD). The CSD is an important parameter because it determines the physical properties of both the wet crystal magma and the dried crystal product in bulk. An inappropriate CSD may result in a reduced performance of downstream solid–liquid separators and may cause caking of the final dried-crystal product, yielding transportability and storage problems. In many cases these problems occur when the mean crystal size is low and when an excessive number of small crystals (*fines*) exists in the distribution.

Inappropriate CSDs may exist (temporarily) due to process disturbances, intrinsic physical feedback mechanisms, which can cause cycling of the CSD, and during plant start-up and shutdown. For these reasons the derivation of accurate (low-order) dynamic models that can be used for CSD controller design is a major issue.

In the literature, experimental results on identification and control of crystallizers are scarce. This is mainly due to a lack of on-line sensors and the absence of reliable experimental equipment, including sampling systems. Miller and Rawlings (1994) present results on parameter estimation within a first-principles model structure, including a method for the estimation of confidence intervals, based on batch crystallization experiments. In earlier work (Eek et al., 1995a), results from first-principles modeling of continuous crystallizers and the estimation of empirical parameter values on the basis of start-up experiments are presented. The experimental data sets were obtained from the free start-up responses of a pilot crystallizer. An overview of identification using first-principles models is given by Rawlings et al. (1993). In general, the derivation of accurate first-principles models will be elaborate in case complicated phenomena such as nonideal mixing, agglomeration, length-dependent growth, and entrance classification due to nonideal sampling occurs. Another difficulty

Correspondence concerning this article should be addressed to P. M. J. Van den Hof.
Current address of R. A. Eek: Bayer AG, ZF-TST, Bldg. E41, D-51368, Leverkusen, Germany.

is that the resulting models generally are nonlinear and have a high order. Thus linearization and model reduction are required for application of these models in model-based controller design, as in, for example, predictive control.

As an alternative to first-principles modeling, system identification is a valuable tool for arriving at low-order linear models directly, without relying heavily on *a priori* knowledge. With multivariable system identification experiments the relevant process dynamics are deliberately excited with uncorrelated, frequency-rich, test signals (Ljung, 1987), which are added to the different process inputs simultaneously. On the basis of the measured input–output data, low-order process models are estimated directly. Results on system identification of crystallization processes were first published by De Wolf and Van den Hof (1992). Their results are, however, limited mainly by limitations in the experimental equipment that was used.

The purpose of this article is to describe a procedure for the identification of low-order models for the dynamics of a continuous crystallization process. We will show that direct identification on the basis of open-loop process data yields poor results, as the process has a tendency to cycle. Applying a simple single-input/single-output (SISO) stabilizing feedback loop, results in a new problem of model identification under closed-loop conditions. To solve this problem consistently, a two-step identification procedure is applied. It is shown that low-order linear models for the process can be accurately estimated at stabilized conditions around the stationary process behavior. The intended use of the resulting models is predictive control.

As a start a short description of the process to be identified is given. Next the results of an open-loop identification experiment are shown. A method for consistent model identification in a closed-loop fashion is described and applied to process data. Finally, the estimated input–output models are validated by an independent data set, and conclusions are drawn with respect to the validity of the applied identification approach.

Process Description

A drawing of the process being studied is provided in Figure 1. The main characteristics are that the crystallizer is a single-stage evaporative crystallizer that is operated continuously at ideal mixed and isothermal conditions, and with a constant effective volume. Further, it is assumed that the product slurry is removed unclassified, that is, each particle has the same probability to enter the product discharge line, irrespective of its size. A fines segregation and destruction system is present for the removal of fines from the crystallizer volume. A forward light scattering technique is applied, on-line, to measure the CSD dynamics in the main crystallizer volume. As process inputs the fines flow Q_f, the product flow Q_p, and the total heat input P_t are taken. The substance system that is used is ammonium sulphate. The volume of the crystallizer is 970 L. The nominal values of the process input parameters are given in Table 1.

The CSD is characterized by a *population density function* $n(x,t)$, which describes the number of particles per unit of slurry and per crystal size as a function of time. First-principles models for crystallization processes generally make up a first-order partial differential equation for the CSD dynamics, an ordinary differential equation for the supersaturation of the mother liquor—as the main driving force in crystallization—and several empirical relations for crystallization kinetics and particle classifiers. For details on the process and a first principal model, we refer to earlier work (Eek et al., 1995a).

Table 1. Nominal Values and Amplitudes of GBN Test Signals

Process Input	u_{nom}	Δu
y_{r1s}, (RUN2)	0.5	0.25
y_{r1s}, (RUN3)	0.5	0.20
Q_p [mL/s]	215	35
P_t [kW]	120	30

The process considered for identification has three output quantities that directly relate to the population density. The first two outputs are calculated from the raw data outputted by a Malvern particle sizer that employs the principle of forward light scattering. This first output is taken equal to the first-principle component of the dynamically varying output vector, which contains the light scattering energy measured from the 31 Malvern detector rings. The first principal component has the important property that it is the linear combination of the 31 output signals that holds the maximum amount of information in terms of energy (see Jolliffe, 1986, for a proof). Application of principal-component analysis to the measured light scattering data further reveals that already 99.5% of the signal energy is held by the first five principal components. The first principal component (denoted as y_{r1} below) is chosen as an output parameter because it is most sensitive for variations in the CSD, and secondly because it happened to be strongly correlated with variations in the fines number density, for which an effective actuator is also present. Note, however, that this result is a characteristic of

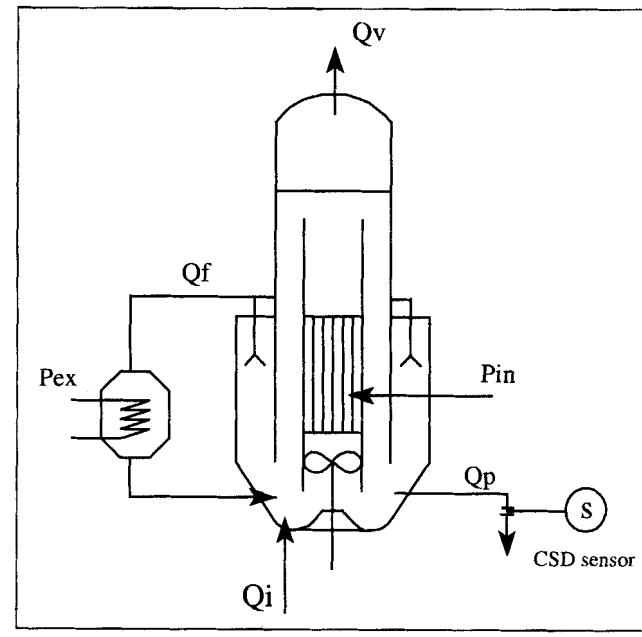

Figure 1. 970-L crystallizer and CSD sensor.

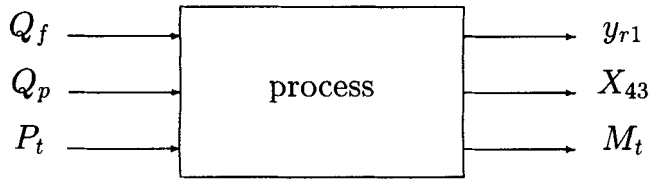

Figure 2. Open-loop process.

the process and sensor applied here. In general, simulation studies using a first-principles model should be conducted to study whether a certain output parameter has the desired characteristics to serve as an input for a controller. An elaborate discussion on the selection of output parameters for stabilizing control of crystallizers is given in Eek et al. (1995b).

As a second output related to the CSD, the mass-based mean crystal size is chosen. This parameter may be used to characterize the efficiency of solid–liquid separation steps in the process downstream. However, depending on the characteristics of a specific application, other CSD-related quantities, such as a measure for the spread or other means, may be better suited. According to a method described in Eek (1995), the mass-based mean crystal size can be estimated from data from the Malvern particle sizer.

The third process output is the magma density of the produced crystal slurry. This process output is related to the third moment of the population density function:
$M_t(t) = \rho_c k_v \int_0^\infty n(x,t)x^3 dx$, where k_v is a shape factor and ρ_c the density of the crystals. Multiplying M_t by the actual product flow gives the yield of the process in produced solids mass per second. In the experimental setup the magma density could be calculated easily from the output of an independent density indicator.

In summary, the (open-loop) process, which will be considered for identification, has three inputs and three outputs. An overview is given by Figure 2. As inputs, we choose the fines flow Q_f, the product flow Q_p, and the total heat input P_t, while as outputs, we choose the number of fines density y_{r1}, the mean crystal size X_{43}, and the magma density M_t.

Open-Loop Plant Behavior

At first the process dynamics were considered by applying excitation signals directly onto the process inputs, in an open-loop fashion. As test signals multisine signals were chosen for the fines removal rate Q_f, and the product removal rate Q_p, each containing 29 logarithmically spaced frequency components. The phase angles of these sinusoids are chosen according to Schroeder (1970), to minimize the signal amplitudes. For every frequency in the first signal the second signal has the first harmonic next to it to obtain uncorrelated signals. In Figure 3, the designed input signals are depicted. A 45-h experiment, which is referred to as RUN1, was performed with the pilot crystallizer. Figure 4 shows the first three principal components of the sensor output, representing 97.1% of the total signal energy. Visual inspection of the data directly reveals that the process output response is strongly dominated by slow cycling behavior of the CSD with a time period of approximately 6 h. Similar observations are reported by Eek (1995). Since the amplitude of this cyclic

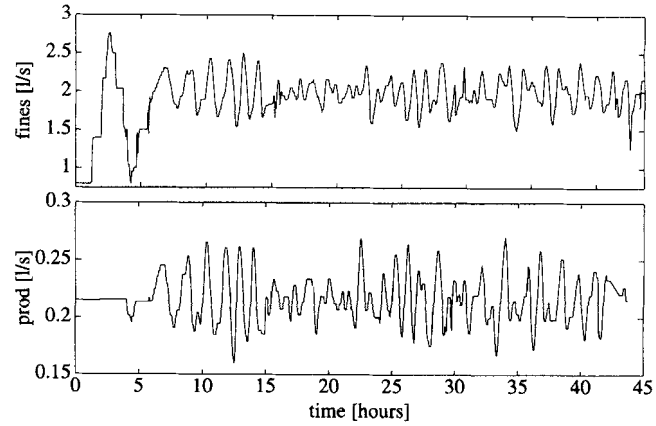

Figure 3. Sinusoidal excitation signals for open-loop identification (RUN1) after $t > 6$ h, for fines flow Q_f (upper) and product flow Q_p (lower).

behavior heavily dominates the effects of input excitation signals in the outputs, it actually takes the process along a range of operating points. Modeling the excited process dynamics by linear models is not appropriate in this situation. From this result it is concluded that for application of a standard linear time-invariant approach for process identification, a closed-loop controller is required that effectively stabilizes the cycling behavior and keeps the process in a fixed operating point during excitation.

Design of a Stabilizing Controller

Simulations with the nonlinear first-principles model described in Eek et al. (1995a) revealed that stability of the CSD can easily be obtained by applying a SISO PI-control loop, which uses the first principal component of the sensor

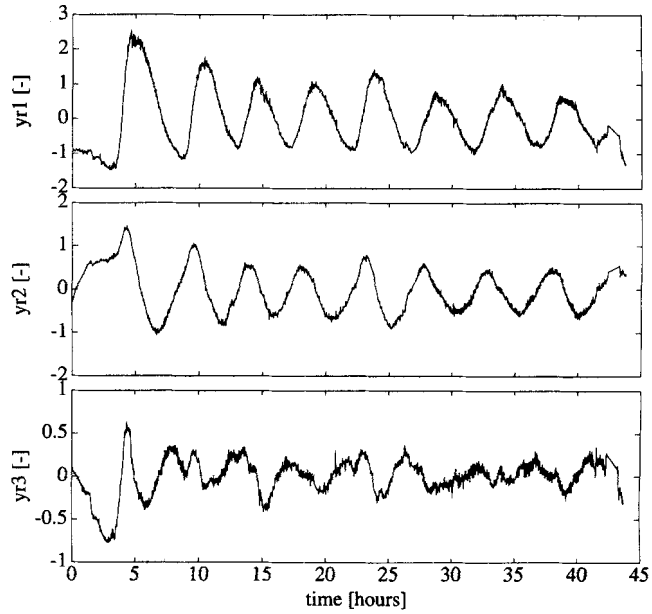

Figure 4. First major three orthogonal signal components obtained with open-loop identification (RUN1); y_{r1} (upper), y_{r2} (middle), y_{r3} (lower).

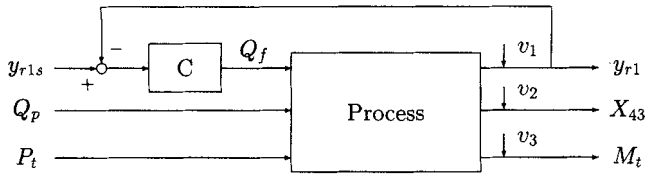

Figure 5. Closed-loop system.

output vector y_{r1} as its input and the fines removal rate Q_f as its output. The feedback control configuration applied here is depicted in Figure 5. Tuning of the controller was also done on the basis of the first-principles model. However, due to the simplicity of the controller, tuning on the pilot plant using simple rules, such as the Ziegler Nichols rules, is a good alternative. The proportional gain of the controller was chosen as 1.0 L/s fines removal for a 100% change in the output signal, and the reset time was chosen as 40 minutes.

Prior to the first closed-loop identification experiment, the ability of the controller to stabilize the startup response of the crystallizer and to follow stepwise setpoint changes was evaluated experimentally. Figure 6 gives the responses of the controlled variable y_{r1}, together with the manipulated variable Q_f, on the process startup and on two setpoint changes at A and B to the controller setpoint. The results indicate that this simple closed-loop configuration effectively dampens open-loop cycling of the CSD and accurately tracks setpoint changes.

Further inspection of the data reveals that the controlled variable has a small offset from the setpoint, which caused a ramplike decrease of the manipulated variable between A and B. A possible explanation for this might be the changing spatial particle concentration, which has gradually lowered the secondary nucleation rate and thereby the fines concentration in the system. Later identification experiments have shown that there is no trend in the data that hinders the parametric identification.

The closed-loop process, which will be considered for further identification, is summarized in Table 2 (see also Figure 5). In addition, following a method that is described in the next section, the controller output Q_f is measured to estimate the open-loop process transfer-functions. The signal y_{r1s} is the setpoint for the stabilizing controller, and $v(t)$ is a noise contribution.

System Identification

The system identification procedure includes the selection of an appropriate model set and a criterion of fit. On the basis of an informative set of process input–output data, the best model within the set is obtained by minimizing the chosen criterion.

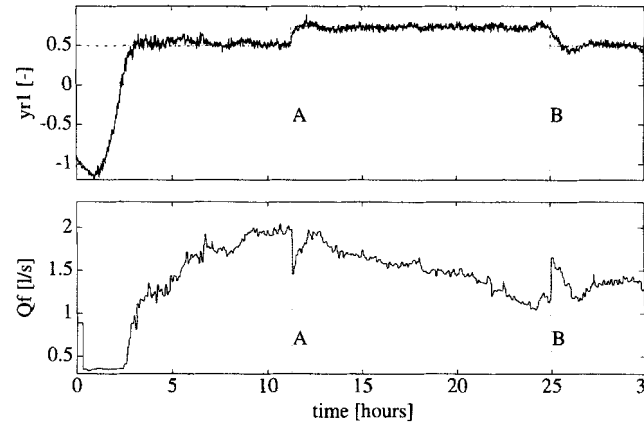

Figure 6. Closed-loop responses to setpoint changes in y_{r1s} (–·–·–) at (A and B) of y_{r1} (upper) and Q_f (lower).

Model structures

Following Ljung (1987) the system to be identified is denoted as

$$y(t) = G_0(q)u(t) + v(t) \tag{1}$$

with $u(t)$, $y(t)$ the process input and output, G_0 a linear time-invariant system represented by its transfer function in the shift operator q, and $v(t)$ a stationary stochastic process represented by $v(t) = H_0(q)e_0(t)$. Here H_0 is the stable and stably invertible noise model, and e_0 is a white noise process. A corresponding model of this process is represented by the collection of transfer functions $[G(q,\theta),\ H(q,\theta)]$, parametrized by some unknown parameter θ, and the corresponding one-step-ahead prediction error is given by

$$\epsilon(t,\theta) = H(q,\theta)^{-1}[y(t) - G(q,\theta)u(t)]. \tag{2}$$

The parametrization of the set of models considered $\{[G(q,\theta),\ H(q,\theta)],\ \theta \in \Theta\}$ can be done in several ways, among which the popular *ARX* parametrization represented by $G(q,\theta) = A(q,\theta)^{-1}B(q,\theta)$ and $H(q,\theta) = A(q,\theta)^{-1}$ with A, B polynomials in the shift operator q^{-1}, leading to the linear regression form:

$$\epsilon(t,\theta) = A(q,\theta)y(t) - B(q,\theta)u(t). \tag{3}$$

An alternative way of parametrizing the models is the output error (OE) form in which the noise model $H(q) = I$ is not parametrized. The input/output model can be represented by a quotient of two polynomials as earlier, but can,

Table 2. Process Inputs and Outputs

Disturbed Inputs	Process Outputs	Output Scale Factor
Controller setpoint, (y_{r1s})	Number of fines, (y_{r1})	1.0
Product flow, (Q_p)	Mean crystal size, (X_{43})	15 μm
Heat input, (P_t)	Magma density, (M_t)	5.1 kg/m^3

for instance, also be parametrized in a FIR (finite impulse response) form:

$$G(q,\theta) = \sum_{k=1}^{n_b} g_k q^{-k}, \tag{4}$$

where the coefficients $\{g_k\}_{k=1,\ldots,n_b}$ are collected in a parameter vector. An alternative form is the state-space model:

$$x(t+1) = A(\theta)x(t) + B(\theta)u(t) \tag{5}$$

$$y(t) = C(\theta)x(t) + D(\theta)u(t). \tag{6}$$

In the latter form the transfer function $G(z)$ is given by $D + C(zI - A)^{-1}B$. To obtain a unique representation of the transfer function within the set of models, the state-space model set is often parametrized in an observable canonical (or pseudocanonical) form; see, for instance, Gevers and Wertz (1987).

Both ARX and OE-FIR models have the advantage that the resulting prediction error is affine in the unknown parameters, leading to a linear regression identification problem. For a least squares identification criterion,

$$\hat{\theta}_N = \arg \min_{\theta \in \Theta} \frac{1}{N} \sum_{t=1}^{N} \epsilon^T(t,\theta)\epsilon(t,\theta), \tag{7}$$

this implies that the estimated parameter can be analytically determined, avoiding numerical nonlinear optimization procedures. Besides, output error model structures in either FIR or state-space form have the advantage that the input/output part $G(q)$ of the model can be consistently identified even if the noise model part $H(q)$ is misspecified (Ljung, 1987).

However, for FIR models the number of parameters to be estimated is generally large, especially when the underlying system dynamics is moderately damped and when the sampling rate is high in relation to the fastest process dynamics. Consequently, the variance of the estimated model parameters will be large as well. A state-space model parametrization does not suffer from this problem; however, the output error to be minimized is a nonlinear function of the model parameters, and the resulting parameter estimate can therefore only be obtained from iterative numerical optimization procedures. Especially for high-order multivariable processes and large data sets, the computational burden can be severe, including possible convergence problems.

As an alternative, there has been renewed interest in the use of generalized (orthogonal) basis functions in a FIR-type model structure:

$$G(z) = \sum_{k=1}^{n_b} b_k f_k(z), \tag{8}$$

where $\{f_k(z)\}_{k=1,\ldots,\infty}$ reflect orthonormal basis functions such as the classic Laguerre functions (see, for instance, Wahlberg, 1991 and Finn et al., 1993), but also more generalized functions generated by freely chosen all-pass transfer functions (Heuberger et al., 1995). In this latter approach a prior knowledge of the process dynamics can be used to flexibly choose the basis functions so as to increase the speed of convergence of the series expansion, Eq. 8. In this way the number of parameters to be estimated can be kept small, while keeping the identified model highly accurate (Van den Hof et al., 1995).

The model structure, Eq. 8, is denoted as ORTFIR. In this article the choice of appropriate basis functions is based on a linearized and reduced first-principles model as well as on estimated ARX models. For all estimated models the OE approach in state-space form was applied as a final step, leading to a numerical nonlinear optimization problem, where the ORTFIR estimated model was used as an initial estimate.

Closed-Loop MIMO Identification

One main and well-known problem related to the identification of a process in a closed-loop configuration is that the noise on the outputs is correlated with the process inputs due to the presence of a feedback loop (see, for example, Figure 2). This correlation generally results in biased estimates for the model, where the bias distribution depends on the characteristics of the noise. Two possible approaches to this problem are employed in this article:

- The direct identification (DI) method. This method fully ignores correlation between inputs and outputs and identifies directly on the basis of closed-loop process input and output data (Söderström and Stoica, 1989).
- The two-step (TS) method as proposed by Van den Hof and Schrama (1993). This approach effectively circumvents correlation problems by subdividing the problem into two successive open-loop identification steps.

Application of the direct approach is straightforward; the TS approach is explained below. For a more detailed presentation, the reader is referred to Van den Hof and Schrama (1993).

Two-step approach

In addition to the process equation (Eq. 1), in a closed-loop setting we have the controller relation:

$$u(t) = r(t) - C(q)y(t) \tag{9}$$

where $r(t)$ is an external reference signal, uncorrelated to the noise disturbance $v(t)$, and $C(q)$ is the controller. Denoting the input sensitivity function

$$S_0(q) = [I + C(q)G_0(q)]^{-1}, \tag{10}$$

it follows that

$$u(t) = S_0(q)r(t) - C(q)S_0(q)v(t). \tag{11}$$

In the first step, using measurement data of $r(t)$ and $u(t)$ one identifies the transfer function S_0. This is an open-loop type of problem, as r and v are uncorrelated. Next the estimate $S(q,\hat{\beta})$ is used to reconstruct a noise-free input signal,

$$\hat{u}_r(t) = S(q,\hat{\beta})r(t), \tag{12}$$

that is used in the second step of the procedure when applying a model structure:

$$\epsilon(t,\theta) = y(t) - G(q,\theta)\hat{u}_r(t). \tag{13}$$

It can be shown that, provided the first step in the procedure is performed accurately enough, this method can provide a consistent estimate of the plant dynamics in the second step. The TS method is applied below to the closed-loop crystallizer data. Another application to a multiinput, multioutput (MIMO) process is reported in Van der Klauw et al. (1994).

Design of a closed-loop experiment

Two closed-loop experiments for identification and successive model validation were conducted with the pilot crystallizer. We refer to these experiments as RUN2 and RUN3. All three inputs of the closed-loop process, for example, y_{r1s}, Q_p, and P_t (see also Figure 5), have been excited with generalized binary noise sequences (GBN), which were introduced by Tulleken (1990). These signals switch (pseudo-) randomly between two fixed signal levels at discrete points in time. Choosing a switching probability between $0.5 < p < 1$ will provide more excitation in the low-frequency range; conversely, choosing $0 < p < 0.5$ will increase the signal energy in the high-frequency range. An important advantage of binary noise sequences is that the energy is roughly evenly distributed over the frequency range of interest, hence the maximum signal amplitude is lower in comparison to multisine excitation. In addition, plant operators are most familiar with stepwise or pulsewise signals.

The basic intervals for the GBN signals here is 20 min. The switching probability was chosen as $p = 0.7$. The real nominal signal values u_{nom} and their amplitudes Δu are given in Table 1. Because the range of the actuators is limited the amplitude of the test signals is limited. The amplitude for the test signal for the setpoint y_{r1s} is determined with the nonlinear simulation model mentioned earlier. In general, when the physical actuator range is limited, the use of GBN signals is preferable, as they give maximum excitation at a low amplitude.

The GBN signal used for RUN2 is sufficiently uncorrelated with the signal for RUN3, while its frequency contents are comparable. A duration of 50 h was chosen for both experiments. This value equals roughly eight times the dominant time constant in the system. Similar identification experiments performed on the nonlinear first-principles model revealed that a fifth-order state-space model could accurately describe the simulation data.

Data Preprocessing. Proper treatment of the data prior to the estimation of parameters is necessary in order to obtain good identification results (Ljung, 1987). The raw process data consist of measured values for the density, and are recorded from the independent density sensor, with a sample time of 10 s, and the scattered light energy vectors, which are sampled with a frequency of one sample per minute. The measured scattered light intensity vectors are averaged values from batches of 1,000 sweeps each, which are recorded from the detector in approximately 5 s.

All scattered light energy patterns were corrected for the signal background (Eek, 1995). The recorded light diffraction patterns are normalized by subdividing each element by the total scattered light energy. Signal outliers are removed by linear interpolation between adjacent measurements. The fines density y_{r1} and the mean crystal size X_{43} are estimated from the normalized diffraction patterns, according to the method described earlier. The nominal values of the mean and the magma density were 600 μm and 1,305 kg/m^3, respectively. The output signals are detrended by removing the best straight line fit from each signal. Detrending is necessary to remove the contribution of process disturbances in the output signal, because this contribution cannot be explained from input variations. To obtain a well-conditioned problem, all input and output signals are scaled and their mean is subtracted, which results in output signals that have equal energy in terms of the signal 2-norm. The original data are sampled too fast for control, so in a final step, the data are filtered and resampled by reducing the sampling rate by a factor of 5. The resulting set of three input and three output signals, each containing 600 data points, is described in Table 2. For interpretation of the scaled signals the scale factors with physical units are added to the same table. The data from RUN3 are used for identification, and those of RUN2 for validation.

Model Verification. A model-verification step is included to judge whether the estimated models are sufficiently accurate. Model verification is done in the time domain on the basis of the independent data set (RUN2). A scalar measure, denoted as the relative mean square (RMS) value, is evaluated for assessing the quality of fit. This measure is calculated from

$$RMS_i = \sqrt{\frac{\sum_{k=1}^{N} [y_i(k) - \hat{y}_i(k)] \times [y_i(k) - \hat{y}_i(k)]}{\sum_{k=1}^{N} y_i(k) y_i(k)}} \tag{14}$$

for each output y_i, $i = 1, 2, 3$, with $\hat{y}_i$ the noise-free simulated output and y_i the measured output. In the frequency domain, models are compared on the basis of their Bode plots.

Results and Discussion

The excitation signals presented in the previous section were used to identify the dynamics of the open-loop process, on the basis of closed-loop data. During the validation experiment (RUN2), a relatively thick concentration of inert gas bubbles was observed in the solution, due to air leakage into the (vacuum) crystallizer. Since these bubbles are observed as particles by the sensor, the observed process trends are likely to be corrupted by this nonquantified disturbance.

Results of direct identification

Three state-space models in canonical observability form, with orders 3, 4 and 5, were estimated directly on the basis of the input–output data from RUN3. Also an initial state and an offset were estimated, while the direct coupling matrix D in Eq. 6 was fixed to zero. Hence in total 24, 31, and 38 parameters were estimated, respectively, on the basis of 600 input–output samples. The RMS values of the estimated

Table 3. RMS Values for y_{r1} (RMS1), X_{43} (RMS2) and M_t (RMS3), of Directly Estimated Models (DI), and the Two-Step Approach (TS), on the Basis of Identification Data (idf), Identification Data with the Model in Closed-Loop (cl), and Validation Data (val)

	RMS1		RSM2		RMS3	
	DI	TS	DI	TS	DI	TS
Third-order model						
idf	0.52	0.54	0.59	0.56	0.28	0.28
cl	0.57	0.55	0.78	0.92	0.30	0.32
val	1.00	1.10	1.29	1.52	0.50	0.55
Fourth-order model						
idf	0.52	0.47	0.51	0.52	0.20	0.28
cl	0.57	0.50	0.86	0.86	0.24	0.29
val	0.99	1.13	1.40	1.42	0.42	0.49
Fifth-order model						
idf	0.45	0.45	0.51	0.46	0.29	0.27
cl	0.51	0.46	0.94	0.67	0.44	0.33
val	0.96	1.24	1.26	1.59	0.52	0.58
Nonlinear model						
idf		0.65		1.17		0.46
val		0.82		1.08		0.58

models, for both the identification (denoted as idf) and the validation (denoted as val) experiment, are given in Table 3. The consistency of the model was checked by again adding the (known) stabilizing feedback controller to the estimated open-loop model and simulating the output response, successively, on the basis of the three (GBN) test signals. The resulting RMS values (denoted as cl) are also provided in Table 3.

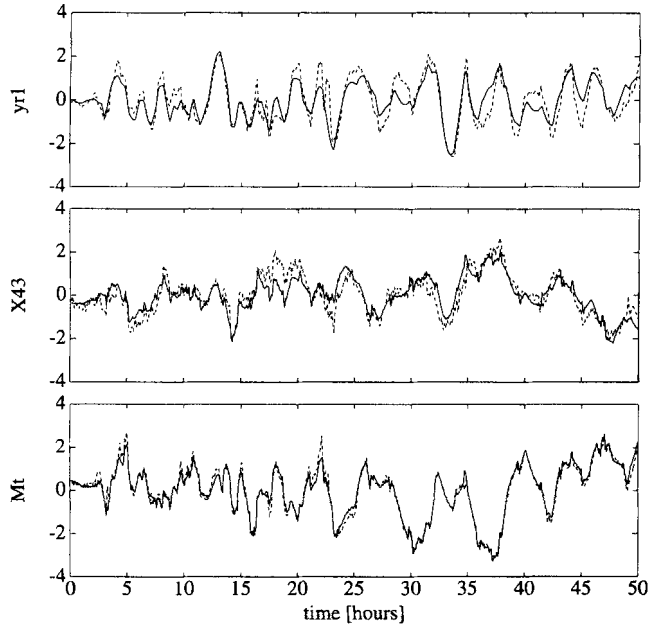

Figure 7. Identification of fourth-order model (——) estimated with direct identification method on data from RUN3 (----); fines density y_{r1} (upper), mean crystal size X_{43} (middle), and magma density M_t (lower).

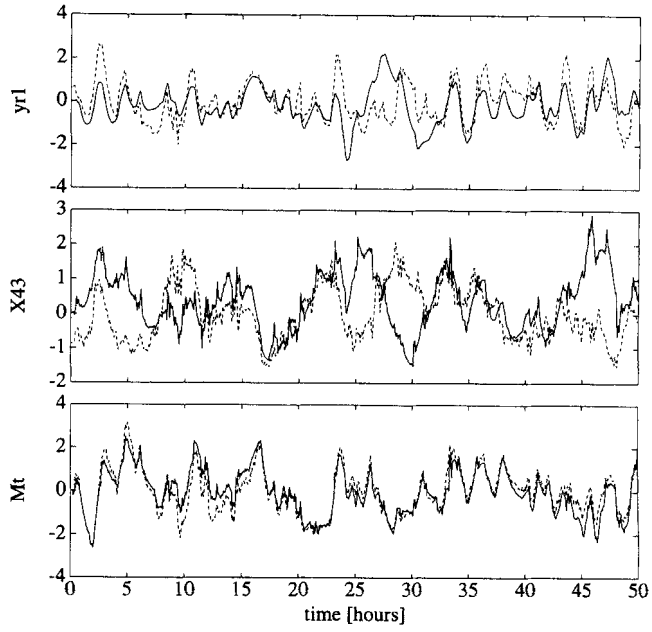

Figure 8. Validation of fourth-order model (——) estimated with direct identification on data from RUN3 (----), with uncorrelated data from RUN2; fines density y_{r1} (upper), mean crystal size X_{43} (middle), and magma density M_t (lower).

Checking the RMS values reveals that the fourth-order model gives the best fit. Figures 7 and 8 show the fit of this model on the identification and the validation data set, respectively. Note that the first portion of the simulated signal trend in Figure 8 is biased, as the initial model state was kept at zero.

The results show a good fit on the identification set. However, some large deviations are present in the validation data set. Particularly between 24 and 32 h large deviations exist. As mentioned before, these deviations may be due to process disturbances, as well as the nonstationary initial state.

Results of two-step identification

Application of the first step of the two-step identification procedure resulted in a sixth-order state-space model in canonical observability form, for the input sensitivity model Eq. 10. Note that all three inputs of the process (Figure 5) had to be used in this step, as all three affect the input Q_f. The known value for the proportional action of the controller was used to determine the coupling matrix D *a priori*. Also an initial state was estimated. A noise-free output signal for the stabilizing controller was simulated with the sensitivity model. The measured and reconstructed output signal of the controller are given in Figure 9. The RMS value, calculated from Eq. 14, corresponding to this fit is 0.25. This plot shows that the difference between the reconstructed and the measured input signal is small. This, however, does not necessarily imply that the result of the second step is equal to the result of the direct identification step. Bode plots of the estimated transfer functions are used below to explore this difference further.

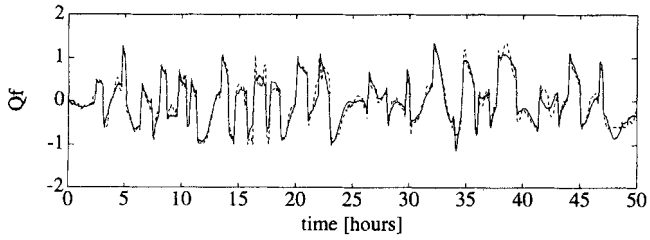

Figure 9. Measured (----) and reconstructed process output signal Q_f (——) of stabilizing controller on the basis of sixth-order estimated state-space model.

In the second identification step, again third-, fourth-, and fifth-order state-space models in canonical observability form were estimated in an open-loop fashion. However, the input signal u is now replaced by the reconstructed signal $\hat{u}_r$, as obtained from the first identification step. An initial state and an offset were also estimated, while the coupling matrix D was kept zero.

The RMS values of the residuals, calculated from Eq. 14, of the different models for both data sets are given in Table 3. Also the estimated open-loop model is simulated in closed-loop on the basis of the excitation signals. The resulting RMS values are provided in Table 3. A fourth-order model also seems to provide the best estimate of the open-loop process dynamics for this case. The fit on the identification set

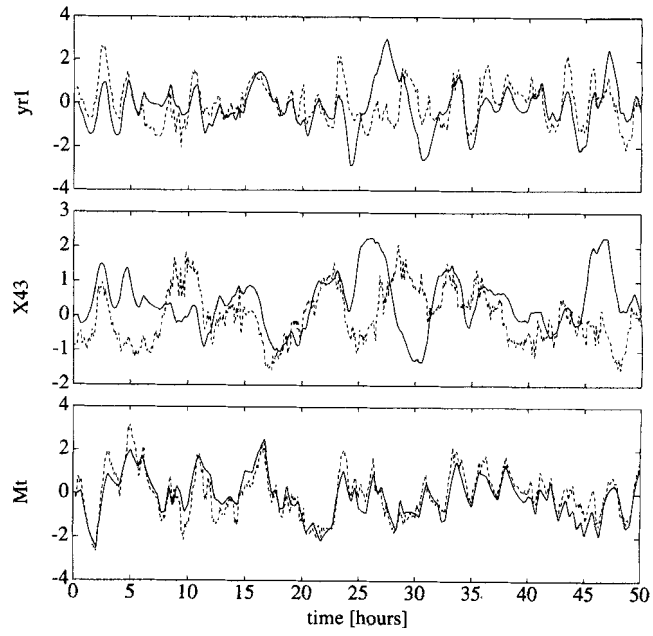

Figure 10. Validation of fourth-order model (——) estimated with two-step identification method on data from RUN2 (----), with uncorrelated data from RUN3; fines density y_{r1} (upper), mean crystal size X_{43} (middle), and magma density M_t (lower).

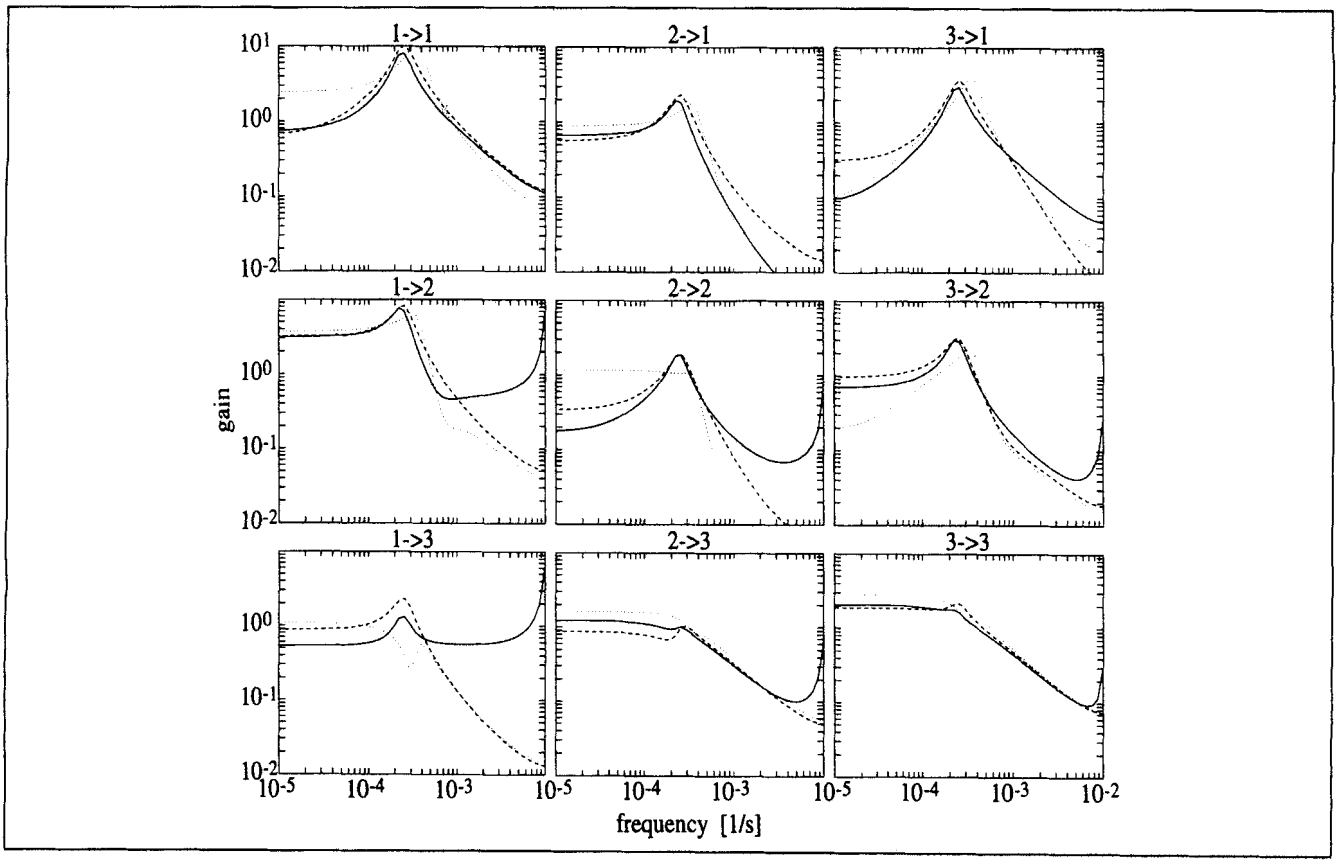

Figure 11. Bode amplitude of fourth-order models obtained from direct approach (——), the two-step approach (----), and the first-principles model (dotted), where $i \rightarrow j$ denotes the transfer relationship of the ith input to the jth output (Figure 1).

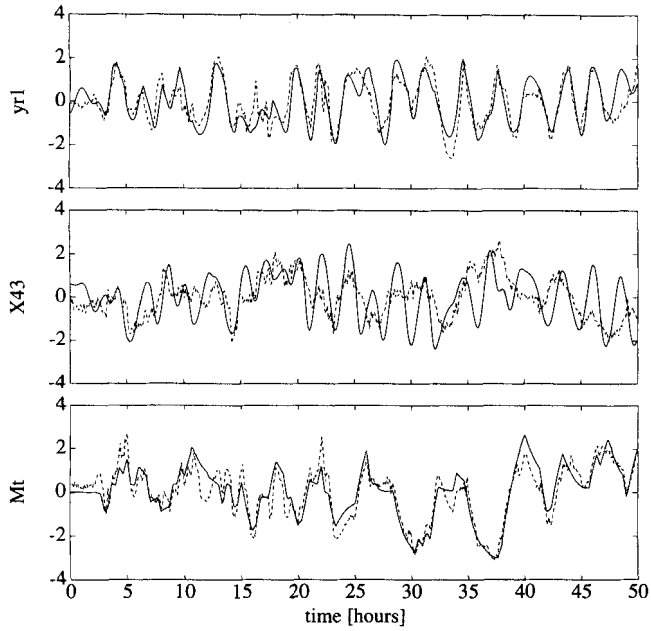

Figure 12. Fit of nonlinear process model (——) on measured data of RUN3 (----); fines density y_{r1} (upper), mean crystal size X_{43} (middle), and magma density M_t (lower).

strongly resembles the fit obtained with the direct approach. Figure 10 shows the fits on the validation sets. At first hand, the RMS values and the time domain fits reveal a small difference between the DI and the TS models. However, if we compare the Bode plots of these models given in Figure 11, a clear difference is observed, mainly in the region of high frequencies. The deviation of the DI model from the TS model exists mainly due to the existence of a correlation in the noise between the input–output signals used in the DI approach. This result confirms the importance of using the proposed TS approach instead of the straightforward DI approach.

Comparison with the first-principles modeling approach

To explore the merits of system identification further, we finally compared the results with a first-principles modeling procedure that was published earlier.

Using the system identification data, we verified the nonlinear process model described in Eek et al. (1995a). It was found that the model with parameters estimated from startup experiments already gave a good description of the data. The fits of the nonlinear model on the identification data set are given in Figure 12, and the RMS values of the output errors are provided in Table 3. The fit on the output y_{r1} is better than the fit on output X_{43}. The latter exhibits a less regular response on the input excitation than the real process trend. Probably a dispersion effect that regularizes the disturbances in the CSD, when they are transported (by crystal growth) over the crystal size domain, is responsible for this. The dynamics of the magma density M_t is described with approximately the same accuracy as with the input–output model. On the basis of the identification data set, the first-principles model does not perform significantly worse or better than the identified model.

In Figure 11, the Bode plot of a fourth-order model obtained by linearizing and reducing the nonlinear model, according to methods described in Eek (1995), is added as a dotted line. As can also be concluded, the linearized and reduced first-principles model strongly resembles the input–output model in the frequency domain. The observed differences in the gain were comparable to the differences in the phase plots. The largest difference is present in the steady-state transfer function. It may be expected that the physical model gives a better description of the low-order dynamics in the system than does the input–output model, because limited information on the steady state is present in the input–output data. It should be noted, however, that a proper estimate of the static gain is less important for most control applications, as most controllers will have integral action, which will compensate effectively for this mismatch.

Since the first-principles model contains significantly fewer unknown parameters, fewer informative process data are needed. Hence, the method may suit industrial requirements better. For many applications, however, the time needed to develop a first-principles model will be greater and necessitate the use of a system identification procedure as described here.

Conclusions

Accurate modeling of CSD dynamics in a crystallization process can be difficult, as many complex phenomena such as nucleation and particle growth are involved. In this article we have shown that system identification is a valuable tool for deriving low-order models for the relevant dynamics of a continuous crystallization process, solely on the basis of input–output data. Identification should be performed in closed-loop to prevent the process outputs from being dominated by a slowly cycling mechanism. Closed-loop stability of the CSD can be achieved with a simple PI controller that uses a signal related to the density of fines as its input and the fines removal rate as its output. Direct identification of input–output models, on the basis of process input–output data with correlated noise, shows that a significant bias in the high-frequency range of the transfer functions is introduced. This consistency problem could be circumvented effectively by a two-step identification procedure. It was found that a fourth-order linear time invariant state-space model can accurately describe the dynamics of the three-input, three-output process. Finally the estimated black-box models are compared with a first-principles model that was published earlier. From this it is concluded that first-principles modeling may be an alternative approach when reliable process input–output data are absent.

Acknowledgments

The authors are indebted to Raymond de Callafon, who implemented the ORTFIR method, and to the Dutch Foundation of Technology (STW), AKZO, DOW Chemicals, DSM, E. I. DuPont de Nemours, and Eastman Chemical Company for their financial support of the UNIAK research program.

Notation

(A, B, C) = state-space model matrices
E = expected value
$\{g_k, b_k\}_{k=0,1,2,\ldots}$ = expansion coefficients

m_i = ith moment of distribution
S = sensitivity function
T = mapping of scattered light to mean size
x = crystal size, m
y_{ri} = ith principle component of Malvern output
β = model parameters

Subscripts

c = controller
e = effective

Literature Cited

De Wolf, S., and P. M. J. Van den Hof, "Identification of a Pilot Plant Crystallization Process with Output Error Methods," *Identification and System Parameter Estimation*, C. Banyasz and L. Keviczky, eds., IFAC Symp. Ser., Vol. 3, p. 133 (1992).

Eek, R. A., "Control and Dynamic Modelling of Industrial Suspension Crystallizers," PhD Thesis, Delft Univ. of Technology, Delft, The Netherlands (1995).

Eek, R. A., Sj. Dijkstra, and G. M. van Rosmalen, "Dynamic Modeling of Suspension Crystallizers, Using Experimental Process Data," *AIChE J.*, **41**, 571 (1995a).

Eek, R. A., S. J. Rusticus, and Sj. Dijkstra, "Design of Robust Stabilizing Feedback Controllers for a Continuous Crystallization Process," *Chem. Eng. Sci.*, submitted (1995b).

Finn, C. K., B. Wahlberg, and B. E. Ydstie, "Constrained Predictive Control Using Orthogonal Expansions," *AIChE J.*, **39**, 1810 (1993).

Gevers, M., and V. Wertz, "Techniques for the Selection of Identifiable Parametrizations for Multivariable Linear Systems," *Control and Dynamic Systems*, Vol. 26, Academic Press, New York, p. 35 (1987).

Heuberger, P. S. C., P. M. J. Van den Hof, and O. H. Bosgra, "A Generalized Orthonormal Basis for Linear Dynamical Systems," *IEEE Trans. Automat. Contr.*, **AC-40**(3), 451 (1995).

Jolliffe, I. T., *Principal Component Analysis*, Springer-Verlag, New York (1986).

Ljung, L., *System Identification*, Prentice-Hall, Englewood Cliffs, NJ (1987).

Miller, S. M., and J. B. Rawlings, "Model Identification and Control Strategies for Batch Cooling Crystallizers," *AIChE J.*, **40**, 1312 (1994).

Rawlings, J. B., S. M. Miller, and W. B. Witkowski, "Model Identification and Control of Solution Crystallization Processes: A Review," *Ind. Eng. Chem. Res.*, **32**, 1275 (1993).

Schroeder, M. R., "Synthesis of Low-Peak Factor Signals and Binary Sequences with Low Autocorrelation," *IEEE Trans. Inform. Theory*, **IT-16**, 85 (1970).

Söderström, T., and P. Stoica, *System Identification*, Prentice-Hall, Englewood Cliffs, NJ (1989).

Tulleken, H. J. A. F., "Generalized Binary Noise Test-Signal Concepts for Improved Identification—Experiment Design," *Automatica*, **25**, 37 (1990).

Van den Hof, P. M. J., and R. J. P. Schrama, "An Indirect Method for Transfer Function Estimation from Closed Loop Data," *Automatica*, **29**, 1523 (1993).

Van den Hof, P. M. J., P. S. C. Heuberger, and J. Bokor, "System Identification with Generalized Orthonormal Basis Functions," *Proc. IFAC Symp. System Identification*, Vol. 3, Copenhagen, Denmark, p. 212 (1994). (Extended version to appear in *Automatica*, **31**(12), 1821 (Dec. 1995).

Van der Klauw, A. C., G. E. van Ingen, A. van Rhijn, S. Olivier, P. P. J. van den Bosch, and R. A. de Callafon, "Closed-Loop Identification of a Distillation Column," *Proc. IEEE Conf. Control Applications*, Glasgow, UK, p. 275 (1994).

Wahlberg, B., "System Identification Using Laguerre Models," *IEEE Trans. Automat. Contr.*, **AC-36**, 551 (1991).

Manuscript received Dec. 8, 1994, and revision received Apr. 17, 1995.